



ARTICLE

Activation of the endocannabinoid system mediates cardiac hypertrophy induced by rosiglitazone

Ya-han Liu¹, Yan Liu¹, Xu Zhang^{1,3}, Li Fang¹, Bei-lei Zhao¹ and Nan-ping Wang²

Rosiglitazone (RSG) is a synthetic agonist of peroxisome proliferator-activated receptor- γ (PPAR γ), which plays a central role in the regulation of metabolism. Meta-analyses have suggested that RSG is associated with increased cardiovascular risk. However, the mechanisms underlying such adverse cardiac effects are still poorly understood. Here, we found that activation of PPAR γ by RSG stimulated the endocannabinoid system (ECS), a membrane lipid signaling system, which induced cardiac hypertrophy. In neonatal rat cardiomyocytes, RSG increased the level of anandamide (AEA); upregulated the expression of N-acyl phosphatidylethanolamine phospholipase D (NapePLD), a key enzyme for AEA synthesis; and downregulated the expression of fatty acid amide hydrolase (FAAH), the enzyme responsible for the degradation of AEA. Importantly, PPAR γ activation increased the expression of cannabinoid receptor type 1 (CB1) through an identified binding site for PPAR γ in the CB1 promoter region. Moreover, both the in vitro and in vivo results showed that inhibition of the ECS by rimonabant, an antagonist of CB1, attenuated RSG-induced cardiac hypertrophy, as indicated by decreased expression of cardiac hypertrophy markers (ANP and BNP), deactivation of the mTOR pathway, and decreased cardiomyocyte size. Thus, these results demonstrated that the ECS functions as a novel target of PPAR γ and that the AEA/CB1/mTOR axis mediates RSG-induced cardiac remodeling.

Key words: peroxisome proliferator-activated receptor- γ ; endocannabinoids; cardiac hypertrophy; mammalian target of rapamycin

Acta Pharmacologica Sinica (2022) 43:2302–2312; <https://doi.org/10.1038/s41401-022-00858-x>

INTRODUCTION

The endocannabinoid system (ECS) is a signaling system mainly composed of two types of cannabinoid receptors (CB1 and CB2); the two most studied endogenous agonists of such receptors, the endocannabinoids (eCBs) anandamide (AEA) and 2-arachidonoylglycerol (2-AG); and the key enzymes regulating the synthesis and degradation of these molecules. The ECS participates in various brain functions in the central nervous system (CNS). In addition to being expressed in the brain, components of the ECS system are also abundantly expressed and exert several important effects in cardiovascular tissues, where they influence various pathophysiological processes [1–3]. Accumulating evidence suggests that aberrant activation of the ECS is linked to different types of cardiac disorders [4, 5]. In aortic stenosis patients, an increased concentration of AEA in cardiomyocytes has been proven to be associated with myocardial hypertrophy [6]. In mouse models, cirrhosis and doxorubicin-induced cardiomyopathy were characterized by increased myocardial AEA levels [7, 8]. Increases in both myocardial AEA levels and CB1 expression were observed in type 1 diabetic cardiomyopathy, contributing to cardiac dysfunction and fibrosis [9]. In addition, blockade of CB1 alleviated left ventricular hypertrophy in mice with chronic kidney disease and improved cardiac contractility in cirrhotic rats [8, 10]. Furthermore, pharmacological inhibition or genetic deletion of CB1 attenuated

diabetes- and doxorubicin-induced cardiac dysfunction [7, 9, 11]. In contrast, activation of CB2 has been shown to exhibit protective effects in many cardiac disorders. Administration of 2-AG or CB2 agonist during ischemia/reperfusion (I/R) in mice improved myocardial recovery, and these cardioprotective effects were abolished by administration of CB2 antagonist [12, 13]. In addition, CB2 deficiency enhanced apoptosis and remodeling after myocardial infarction (MI), leading to ventricular dysfunction and exacerbation of fibrosis [14, 15].

Thiazolidinediones (TZDs), such as rosiglitazone (RSG) and pioglitazone (PIO), are high-affinity ligands for peroxisome proliferator-activated receptor γ (PPAR γ), which is a member of the PPAR nuclear receptor superfamily. TZDs are insulin sensitizers and have been successfully used in the clinical treatment of type 2 diabetes [16, 17]. When PPAR γ is activated by TZDs, it regulates countless downstream genes involved in multiple critical biological processes, including cardiac metabolism, function, and structure [18]. In the past decades, a large body of emerging evidence has suggested that RSG is associated with increased cardiovascular risk, especially for heart failure events [19–22]. Although the trials of pioglitazone indicated mostly positive effects, reporting a lower risk of stroke and MI, it is worth noting that in some reports, pioglitazone appeared to increase the risk of edema and congestive heart failure (CHF) [23]. In rodent models, either RSG treatment or PPAR γ overexpression can induce cardiac hypertrophy, which is an

¹Key Laboratory of Molecular Cardiovascular Science, Ministry of Education; Institute of Cardiovascular Sciences, Peking University Health Science Center, Beijing 100191, China and ²East China Normal University Health Science Center, Shanghai 200241, China

Correspondence: Nan-ping Wang (nanpingwang2003@yahoo.com)

³Present address: Tianjin Key Laboratory of Metabolic Diseases, Department of Physiology and Pathophysiology, Tianjin Medical University, Tianjin 300070, China

Received: 15 August 2021 Accepted: 3 January 2022

Published online: 21 February 2022

important pathophysiologic step in the development of heart failure [24–29]. However, the mechanisms underlying the hypertrophic effects of RSG are incompletely known.

In addition to TZDs, the synthetic ligands of PPAR γ , natural PPAR γ ligands include polyunsaturated fatty acids such as arachidonic acid and its metabolites. Recent accumulating evidence indicates that eCBs and endocannabinoid-like compounds can also bind directly to and activate PPAR γ , mediating several physiological effects. AEA can induce PPAR γ transcriptional activation and promote adipocyte differentiation [30, 31]. Elevation of the AEA level by inhibition of its degradation or transport potentiates the LPS-induced increase in the circulating TNF- α level, which can be blocked by PPAR γ antagonist [32]. In the cardiovascular system, a PPAR γ -sensitive vasorelaxant response in the aorta has been observed in response to AEA [33]. It has also been reported that PPAR γ is an intracellular target of 2-AG and mediates the suppression of IL-2 production by 2-AG in Jurkat T cells [34]. In models of Alzheimer's disease, 2-AG performs a neuroprotective function by inhibiting β -amyloid formation via PPAR γ [35]. Here, we sought to determine whether PPAR γ and ECS can reciprocally regulate each other. To explore the potential mechanisms of ECS–PPAR γ interactions, based on that both the ECS and PPAR γ play important roles in regulating cardiac dysfunction, we tested the hypothesis that ECS activation mediates the cardiac hypertrophic effects of PPAR γ .

MATERIALS AND METHODS

Reagents and cells

Rosiglitazone (RSG) was obtained from GlaxoSmithKline (Brentford, Middlesex, United Kingdom). Pioglitazone (PIO), 2-AG, rimonabant, AM251, SR144528, URB597, and AM630 were purchased from Cayman (Ann Arbor, MI, USA). AEA and oleamide were obtained from Sigma-Aldrich (St. Louis, MO, USA). Rat neonatal cardiomyocytes (NCMCs) and cardiac fibroblasts were isolated from neonatal rat hearts as previously described and cultured in Dulbecco's modified Eagle's medium (DMEM) containing 10% fetal bovine serum (FBS) [36]. Briefly, ventricles of 1- to 3-day-old Sprague–Dawley (SD) rats were cut into 1 mm³ piece and digested in PBS containing 0.1% trypsin (Invitrogen, Carlsbad, CA, USA) and 0.05% type I collagenase (Invitrogen) under constant stirring at 37 °C for 6 min, and the supernatants were then collected. The digestion cycle was repeated until the ventricle pieces became very small and turned white. Cells were pelleted and resuspended in DMEM containing 10% FBS and were then plated in culture dishes. After 2 h, unattached cells were harvested, counted, and plated as a confluent monolayer in new culture dishes. The adherent cells, being considered as cardiac fibroblasts, were gently washed with pre-warmed culture medium to remove unattached cells and debris, and then fresh complete medium was added.

Cell treatment

To determine the effects of TZDs on the ECS, cardiomyocytes or cardiac fibroblasts were subjected to treatment with RSG (1 or 20 $\mu\text{mol} \cdot \text{L}^{-1}$) or PIO (20 $\mu\text{mol} \cdot \text{L}^{-1}$) for 4–48 h. To investigate whether activation of the ECS is mediated by PPAR γ , cardiomyocytes were pretreated with GW9662 (40 $\mu\text{mol} \cdot \text{L}^{-1}$) for 2 h and were then treated with RSG (20 $\mu\text{mol} \cdot \text{L}^{-1}$) for 24 h. To test the hypertrophic effect of eCBs on NCMCs, cardiomyocytes were treated with AEA (10 $\mu\text{mol} \cdot \text{L}^{-1}$) or OEA (50 $\mu\text{mol} \cdot \text{L}^{-1}$) for 24 h or 48 h or were pretreated with the CB1 antagonist rimonabant (3 $\mu\text{mol} \cdot \text{L}^{-1}$) for 2 h and were then treated with AEA (10 $\mu\text{mol} \cdot \text{L}^{-1}$) for 24 or 48 h. To test the hypothesis that CB1 but not CB2 mediates RSG-induced cardiac hypertrophy, cardiomyocytes were preincubated with a CB1 antagonist (rimonabant, 3 $\mu\text{mol} \cdot \text{L}^{-1}$ or AM251, 5 $\mu\text{mol} \cdot \text{L}^{-1}$), or a CB2 antagonist (SR144528, 1 $\mu\text{mol} \cdot \text{L}^{-1}$ or AM630, 1 $\mu\text{mol} \cdot \text{L}^{-1}$) for 2 h and were then treated with RSG (20 $\mu\text{mol} \cdot \text{L}^{-1}$)

for 24 or 48 h. To investigate the effect of inhibition of FAAH on the levels of AEA and 2-AG, cardiomyocytes were treated with FAAH inhibitor URB597 (10 $\mu\text{mol/L}$) for 24 h.

Animal experiments and sample collection

All animal experiments followed the guidelines of the National Institute of Health and were approved by the Institutional Animal Care and Use Committee. SD rats (8 weeks old) were housed under specific pathogen-free (SPF) conditions with ad libitum access to water and a standard laboratory diet throughout the experiments. Rats were treated with RSG (15 $\text{mg} \cdot \text{kg}^{-1} \cdot \text{d}^{-1}$) or vehicle [aqueous solution containing 2% Tween 80 (*w/v*) and 0.5% methylcellulose (*w/v*)] [37] by intragastric gavage (i.g) daily for 2 weeks as previously described [38]. For rimonabant (Rimo) treatment, Rimo (10 $\text{mg} \cdot \text{kg}^{-1} \cdot \text{d}^{-1}$) was administered together with RSG via intragastric gavage for 4 weeks. The body weight was measured weekly. Rats were euthanized by intraperitoneal injection of an overdose of pentobarbital sodium (200 $\text{mg} \cdot \text{kg}^{-1}$). The hearts were rapidly removed, dried on filter paper, weighed, snap-frozen in liquid nitrogen, and stored at -80 °C. For protein and mRNA analysis, ventricular tissues were homogenized with a TissueLyser II (QIAGEN, Germantown, MD, USA).

Western blot analysis

Protein samples were extracted with RIPA buffer containing protease and phosphatase inhibitor cocktail. Protein samples were separated by 12% sodium dodecyl sulfate–polyacrylamide gel electrophoresis (SDS–PAGE) and transferred to polyvinylidene difluoride (PVDF) membranes, and the membranes were incubated with primary antibodies against CB1 (Abcam, Cambridge, MA, USA), mTOR, phosphorylated mTOR and 4EBP1 (Cell Signaling Technology, Beverly, MA, USA). Subsequently, the membranes were incubated with the corresponding HRP-conjugated secondary antibodies, and immunoreactions were detected by chemiluminescence [39].

Quantitative reverse transcription–polymerase chain reaction (qRT–PCR)

Total RNA was extracted from cells or tissues with TRIzol reagent and reverse transcribed into cDNA. Quantitative PCR was performed with GoTaq[®] qPCR Master Mix (Promega, Madison, MI, USA) in an Mx3000P qPCR system (Agilent, Santa Clara, CA, USA). Please see the supplemental materials for the primer sequences (Supplemental Table 1).

Chromatin immunoprecipitation (ChIP) assay

NCMCs were treated with RSG (20 $\mu\text{mol} \cdot \text{L}^{-1}$) for 24 h and were then incubated with formaldehyde to crosslink DNA and proteins. Cells were harvested, and the fixed chromatin was sheared into fragments with an average size of 500 bp (range, 200 to 1000 bp) by sonication. The lysates were incubated with 2 μg of an anti-PPAR- γ antibody (Santa Cruz Biotechnology, Dallas, TX, USA) or control rabbit IgG, and the complexes were then precipitated by using protein A/G agarose beads. The immunoprecipitated products were extensively washed. DNA was purified by using a QIAGEN PCR purification kit and amplified with primers flanking the putative PPAR-responsive element (PPRE) [38] (nucleotides 4811–4823, forward: 5'-CGCGCATGATTAACGG-3' and reverse: 5'-TGTGTCATCCTCACTCTCTG-3').

Measurement of endocannabinoid levels

The levels of AEA and 2-AG in NCMCs were quantified by liquid chromatography–mass spectrometry (LC–MS) [40]. The values are expressed as pmol per 10⁶ cells. NCMCs were homogenized in 2 mL of a 1:1 mixture of cold methanol and acetonitrile containing AEA-d8 and 2-AG-d8 as internal standards (ISs). The homogenates were centrifuged at 4 °C (14,000 $\times g$ for 20 min), and the

supernatants were collected and transferred to clean tubes. Then, the supernatants were evaporated to dryness under nitrogen and resuspended in 100 μL of $\text{MeOH:H}_2\text{O}$ (70:30, v/v) solution [41]. The LC system used for analysis was a Waters Acquity UPLC system (Waters Corporation, MA, USA). Liquid chromatographic separation of eCBs was achieved by using a Waters BEH C18 column (2.1 \times 50 mm, 1.7 μm , 130 \AA) at 30 $^\circ\text{C}$. Mobile phase A consisted of H_2O with 0.1% formic acid. Mobile phase B consisted of acetonitrile with 0.1% formic acid. Gradient elution was performed at a flow rate of 600 $\mu\text{L} \cdot \text{min}^{-1}$, and the injection volume was 10 μL . The initial composition of the gradient was 50% B and was held isocratically for the first half-minute. Then, the concentration of mobile phase B was increased to 80% B over 5 min and was held constant for 1 min. At 6.5 min, the concentration was returned to the initial condition of 50% B to reequilibrate the column. The total run time was 7 min. The UPLC system was connected to a 5500 QTRAP hybrid triple quadrupole/linear ion trap mass spectrometer (AB Sciex, Foster City, CA) equipped with a turbo ion spray electrospray ionization source. The ion source parameters were as follows: CUR = 40 psi, GS1 = 30 psi, GS2 = 30 psi, ISV = 4500 V, CAD = MEDIUM, and TEMP = 500 $^\circ\text{C}$. eCBs were detected by multiple reaction monitoring (MRM) in positive ion mode. The MRM transitions for the eCBs are listed in the following table.

Analyte	Q1	Q3
AEA	348.1	62.1
OEA	326.1	62.1
PEA	300.1	62.1
2-AG	379.1	287.3
AEA-d8	356.3	62.9
2-AG-d8	387.3	105.1

The amounts of AEA and 2-AG in the samples were confirmed by comparison of the precursor and product ion m/z values and LC retention times with those of the standards and were quantified by stable isotope dilution. The obtained peak area was divided by the IS peak area, and the ratio was then compared with the nominal concentration to construct a calibration curve for each metabolite using the least-squares method. The relative levels of PEA and OEA were determined by comparing the peak areas [41].

Metabolic profiling by gas chromatography–mass spectrometry (GC–MS)

Myocardial samples were pulverized into a fine powder in liquid nitrogen with a mortar and pestle. Fifty milligrams of the powder was transferred to an Eppendorf tube, drawn into 50 μL of distilled water and vortexed vigorously for 30 s. Stable isotope-labeled 1,2- $^{13}\text{C}_2$ -myristic acid was added as an internal standard (IS) and was then vortexed for 30 s. After the addition of 900 μL of methanol, the mixture was fully homogenized in a Retsch MM 400 Mixer Mill and was then centrifuged at 20,000 $\times g$ for 10 min at 4 $^\circ\text{C}$. Sixty microliters of the supernatant were transferred to a GC vial and evaporated to dryness under a vacuum. Thirty microliters of methoxyamine in pyridine (10 $\text{mg} \cdot \text{mL}^{-1}$) were added to the GC vial and vortexed for 3 min, and the methoximation reaction was carried out for 16 h at room temperature. Then, 30 μL of MSTFA (with 1% TMCS) was added for trimethylsilylation for another 1 h. Finally, 30 μL of heptane containing the external standard methylmyristate was added to the GC vial.

Metabolic profiling was conducted on a GC/TOF-MS system consisting of an Agilent 69800A gas chromatograph equipped with an Agilent 7683 Series autosampler connected to a Pegasus

III TOF-MS analyzer (Leco, MI, USA). The GC oven temperature was programmed to begin at an initial temperature of 70 $^\circ\text{C}$ (2 min), which was then increased to 305 $^\circ\text{C}$ at 35 $^\circ\text{C} \cdot \text{min}^{-1}$ and maintained for 2 min. The temperatures of the injection port, transfer interface, and ion source were set to 250, 250, and 200 $^\circ\text{C}$, respectively. The selected mass range was set to 50–800 m/z with electron impact ionization (70 eV). Automatic peak detection and calculation of the peak areas of the IS and detected compounds were performed using ChromaTOF 2.00 software by Leco Corporation. Multivariate data analysis and modeling were performed with SIMCA-P 11 software (Umetrics, Umeå, Sweden) [42].

Adenoviral infection

The adenovirus (Ad) expressing constitutively active PPAR γ was described previously [43]. For adenovirus-mediated gene transfer, confluent NCMCs were infected with adenoviruses for 2 h (NCMCs were coinfecting with Ad-tTA to induce tetracycline-controllable expression). After the viral particles were removed by washing, the infected cells were further incubated for the indicated time in the presence or absence of tetracycline. Overexpression of PPAR γ was achieved by infection of NCMCs with Ad-PPAR γ and Ad-tTA and was switched off by the addition of tetracycline to the culture medium.

Evaluation of cardiomyocyte hypertrophy

NCMCs were fixed with 4% (w/v) paraformaldehyde (PFA) for 10 min at room temperature. Then, phalloidin-rhodamine (1:500, Abcam) was added and incubated at room temperature for 1 h. After rinsing three times with PBS, the cells were counterstained with 4,6-diamidino-2-phenylindole (DAPI). Digital images were acquired using a Leica TCS SP8 confocal laser scanning microscope. Image J software was used to quantify the area of cardiomyocytes. At least 100 cells from randomly selected fields were analyzed.

Histological assessment of cardiac hypertrophy

The heart was rapidly removed from each mouse and was then fixed with 4% (w/v) PFA, processed routinely, and embedded in paraffin. Sections were sliced at a thickness of 5 μm . The sections were stained with hematoxylin and eosin (H&E) for histopathological examination. All sections were evaluated by light microscopy.

Statistical analysis

Data analysis was performed using Prism version 8.0 (GraphPad Software, San Diego, CA, USA). The results are expressed as the mean \pm SEM values. Two-tailed Student's t test was performed to analyze the significance of differences between two groups. One-way and two-way ANOVA with significant difference *post-hoc* tests were used to evaluate the statistical significance of differences among more than two groups. P values of <0.05 were considered statistically significant.

RESULTS

Myocardial metabolic alterations in mice treated with RSG

To explore the broad changes in the metabolic profile of mice treated with rosiglitazone (RSG, 15 $\text{mg} \cdot \text{kg}^{-1} \cdot \text{d}^{-1}$), metabolites were extracted from cardiac tissue and analyzed by using GC–MS. Cross-validated OPLS-DA score plots generated from the relative levels of cardiac metabolites discriminated RSG-treated mice (red circles) from control mice (black squares) ($P = 0.047$) (Fig. S1a). Oleamide was a statistically significant metabolite and is highlighted by the circle in the S -plot (Fig. S1b). Fig. S1c shows that the oleamide level was increased 2-fold in RSG-treated cardiac tissues, accompanied by decreased levels of ethanolamine, the metabolic product of eCBs. Oleamide is an endocannabinoid-like molecule

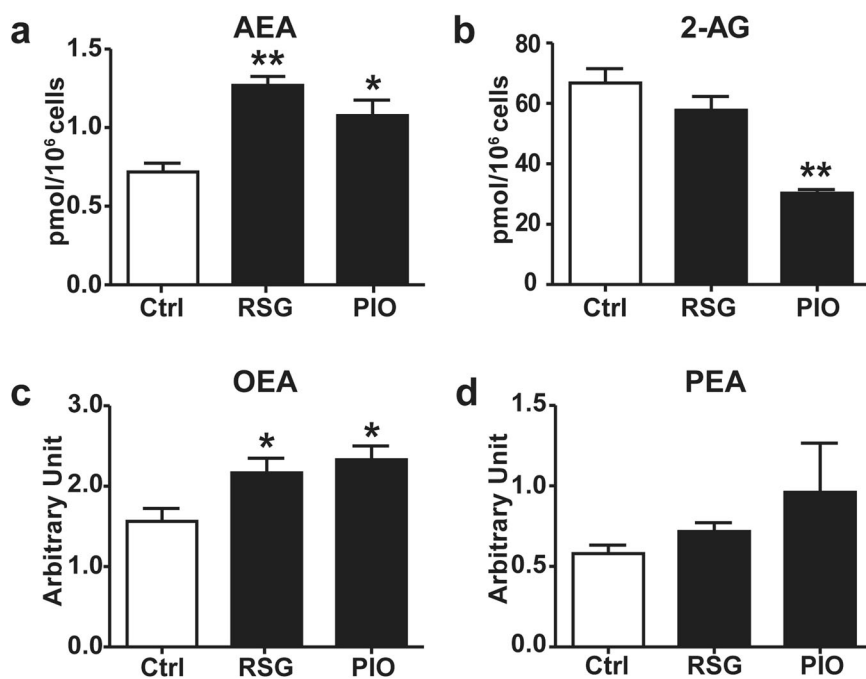


Fig. 1 TZDs regulated the levels of eCBs in cardiomyocytes. The levels of eCBs in per 10⁶ NCMCs after RSG (20 $\mu\text{mol} \cdot \text{L}^{-1}$) and PIO (20 $\mu\text{mol} \cdot \text{L}^{-1}$) treatment for 24 h. **a, b** AEA and 2-AG were assayed by LC–MS with a standard curve, and **c, d** the relative intensity of the ions (arbitrary units) of OEA and PEA were acquired by comparing peak area. Data are mean \pm SEM. * $P < 0.05$, ** $P < 0.01$ vs. Ctrl from one-way ANOVA followed by Sidak's *post hoc* tests. $n = 4$.

that can activate the cannabinoid receptor CB1 and has been reported to serve as a competitive substrate for the enzyme fatty acid amide hydrolase (FAAH), which inhibits degradation of the eCB AEA [44]. Hence, we hypothesized that the ECS, composed of eCBs, their receptors and related metabolic enzymes, can be regulated by PPAR γ agonists.

Thiazolidinediones regulated the levels of eCBs in cardiomyocytes To determine the effects of PPAR γ activation on the ECS, we first tried to measure changes in eCB levels in cardiomyocytes after RSG treatment. By using LC–MS, we developed a method that successfully detected the absolute levels of AEA and 2-AG and the relative levels of oleoylethanolamide (OEA) and palmitoylethanolamide (PEA) in neonatal rat cardiomyocytes (NCMCs). RSG increased the level of AEA by 2-fold but did not significantly affect the level of 2-AG (Fig. 1a). Similarly, pioglitazone (PIO), another thiazolidinedione (TZD) drug, increased the level of AEA but decreased the level of 2-AG (Fig. 1b). In addition, the levels of two eCBs like mediators—OEA and PEA—that are degraded via the same pathway as AEA were increased by both RSG and PIO treatment in cardiomyocytes (Fig. 1c, d).

RSG activated the ECS in cardiomyocytes

We focused on AEA, whose level was elevated by TZD stimulation, by investigating the expression of key enzymes regulating its synthesis or degradation. The precursor of AEA is N-arachidonoyl phosphatidylethanolamine (NAPE), which can be cleaved by a specific phospholipase D (NapePLD) to release AEA. Inactivation of AEA is mediated mainly by cellular uptake followed by hydrolysis into ethanolamine and arachidonic acid via FAAH [45]. We treated cardiomyocytes with 1 or 20 $\mu\text{mol} \cdot \text{L}^{-1}$ RSG and extracted mRNA at different time points. The results showed that the mRNA expression level of NapePLD was increased by RSG (20 $\mu\text{mol} \cdot \text{L}^{-1}$) after 24 h of treatment. In contrast, the mRNA level of FAAH was decreased by RSG. In addition to the expression of the key enzymes, the expression of the receptors in the ECS was also examined. CB1 was upregulated by RSG (20 $\mu\text{mol} \cdot \text{L}^{-1}$) at all time

points. This increased expression was confirmed by analysis of the protein level of CB1 in RSG-treated NCMCs (Fig. 2a–d). However, CB2 expression was not affected by RSG (Fig. S2a). Similar to RSG, PIO, another PPAR γ agonist in the TZD family, also downregulated FAAH mRNA expression and upregulated CB1 mRNA expression (Fig. 2e). In addition, RSG did not have a significant effect on the evaluated ECS components in cardiac fibroblasts (Fig. S2b). Consistent with these findings, in our animal model, oral administration of RSG (15 $\text{mg} \cdot \text{kg}^{-1} \cdot \text{d}^{-1}$) for 2 weeks increased NapePLD and CB1 expression and decreased FAAH expression in the ventricular tissues of rats (Fig. 2f, g). FABP4, a known target of PPAR γ , was included as a positive control. This evidence from both in vitro and in vivo models demonstrated that the ECS is activated by RSG in cardiomyocytes.

Activation of the ECS was mediated by PPAR γ in cardiomyocytes Considering the off-target effect of RSG on the cardiovascular system [46, 47], we used GW9662, an antagonist of PPAR γ , to prove whether the activating effect of RSG on the ECS is dependent on PPAR γ . Pretreatment with GW9662 (40 $\mu\text{mol} \cdot \text{L}^{-1}$) for 2 h inhibited RSG-increased both the mRNA and protein expression levels of CB1. It also attenuated the RSG-induced changes in the mRNA expression levels of NapePLD and FAAH, which reflected the changes in the level of AEA in cardiomyocytes. In addition, the activation of FABP4, a well-known target gene of PPAR γ , was inhibited by GW9662 (Fig. 3a–c). Similar to RSG, adenovirus-mediated expression of constitutively active PPAR γ induced ECS activation by regulating the mRNA expression levels of the genes mentioned above (Fig. 3d). In addition, we characterized the putative PPREs in the RSG-regulated genes involved in the ECS. Bioinformatic analysis using JASPAR predicted one putative binding site for PPAR γ in the 5'-flanking region of the rat CB1 gene. The ChIP assay confirmed that PPAR γ bound to this site (Fig. 3e).

eCBs exerted hypertrophic effects on NCMCs via CB1

We tested whether eCBs have direct hypertrophic effects on NCMCs, based on the expression of two cardiac hypertrophy

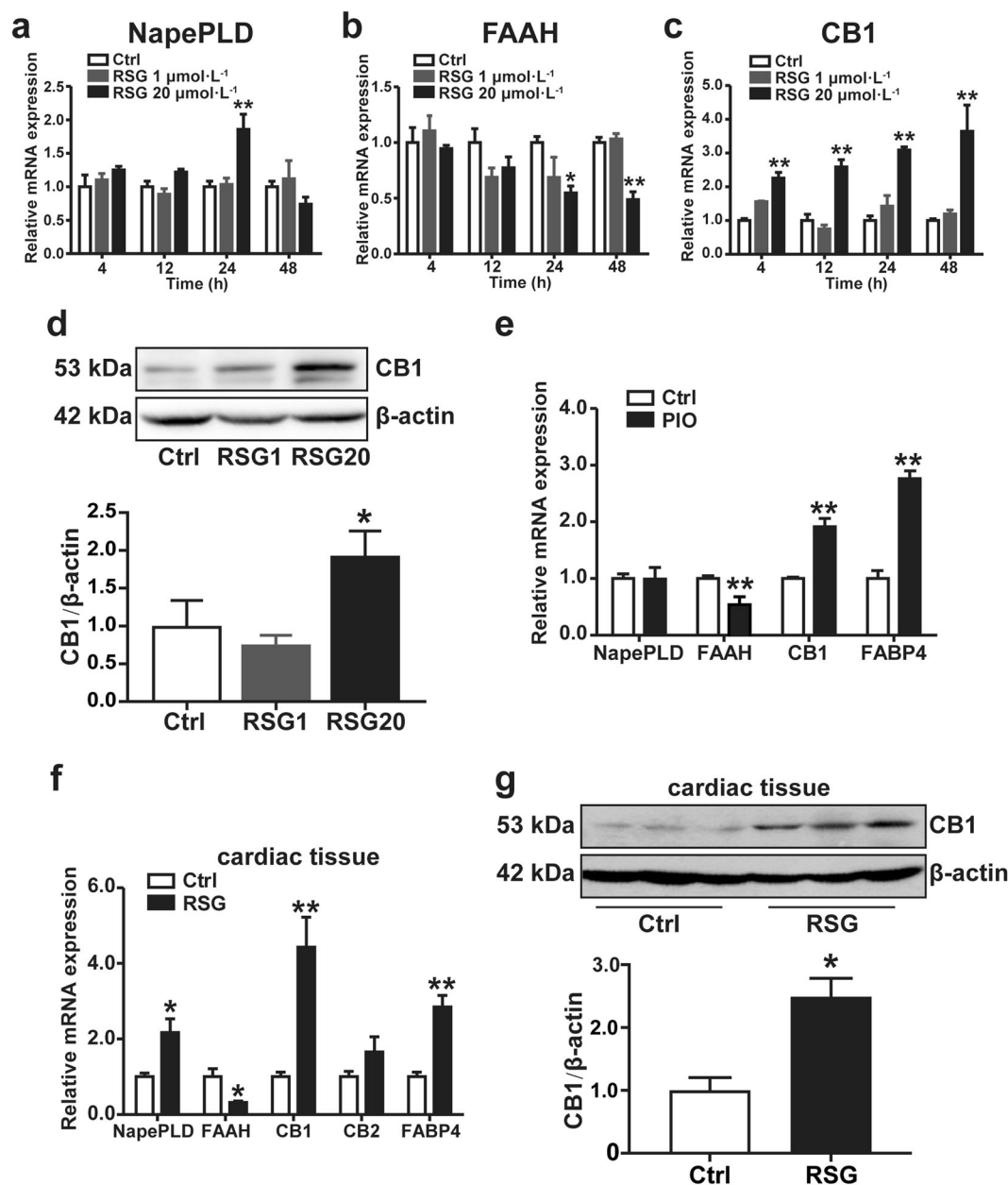


Fig. 2 RSG activated ECS in cardiomyocytes. NCMCs were treated with RSG at 1 or 20 $\mu\text{mol}\cdot\text{L}^{-1}$. mRNA was harvested after indicated time periods. **a–c** The relative mRNA expression levels of NapePLD, FAAH, and CB1 were measured. Data are mean \pm SEM. $*P < 0.05$, $**P < 0.01$ vs. Ctrl from two-way ANOVA followed by Sidak's *post hoc* tests. $n = 3–4$. RSG1, RSG 1 $\mu\text{mol}\cdot\text{L}^{-1}$; RSG20, RSG 20 $\mu\text{mol}\cdot\text{L}^{-1}$. **d** The protein level of CB1 was measured in NCMCs with RSG treatment for 48 h. Data are mean \pm SEM. $*P < 0.05$ vs. Ctrl from one-way ANOVA followed by Sidak's *post hoc* tests. $n = 4$. **e** NCMCs were treated with PIO (20 $\mu\text{mol}\cdot\text{L}^{-1}$) for 24 h, the relative mRNA expression of NapePLD, FAAH, CB1, and FABP4 was measured by qPCR. Data are mean \pm SEM. $*P < 0.05$, $**P < 0.01$ vs. Ctrl from *t*-test. $n = 3–6$. For in vivo study, rats were treated with RSG (15 $\text{mg}\cdot\text{kg}^{-1}\cdot\text{d}^{-1}$) by gavage for 2 weeks. **f** The mRNA expression of genes related to ECS and **g** the protein level of CB1 were measured in cardiac tissue from the left ventricle. Data are mean \pm SEM. $*P < 0.05$, $**P < 0.01$ vs. Ctrl from *t*-test. $n = 3–4$.

markers [atrial natriuretic peptide (ANP) and type B natriuretic peptide (BNP)], cell morphology, and activation of the mTOR pathway. NCMCs were treated with AEA (10 $\mu\text{mol}\cdot\text{L}^{-1}$) or OEA (50 $\mu\text{mol}\cdot\text{L}^{-1}$) for 24 h. The qPCR results showed that AEA increased the mRNA expression levels of both ANP and BNP (Fig. 4a) and that OEA induced only ANP expression. F-actin in NCMCs was stained with rhodamine-conjugated phalloidin to measure the cell surface area. Cardiomyocyte enlargement was observed in the AEA-treated group (Fig. 4b). These data were consistent with previous studies showing that activation of CB1, as the receptor for AEA, mediates cardiac hypertrophy in several cardiac disorders [9, 10]. We found that inhibition of CB1

using the specific antagonist rimonabant (Rimo, 3 $\mu\text{mol}\cdot\text{L}^{-1}$) attenuated AEA-induced expression of ANP and BNP (Fig. 4c). In addition, Rimo inhibited AEA-stimulated phosphorylation of mTOR and 4EBP1 (Fig. 4d). These results supported the hypothesis that AEA can stimulate cardiac hypertrophy through CB1.

Inhibition of CB1 attenuated RSG-induced cardiac hypertrophy in vitro and in vivo
Here, we investigated the role of the ECS in the hypertrophic effect of RSG. NCMCs were treated with different doses of RSG (0, 0.1, 1, 20, 100 $\mu\text{mol}\cdot\text{L}^{-1}$) for 24 or 48 h. The results showed that RSG

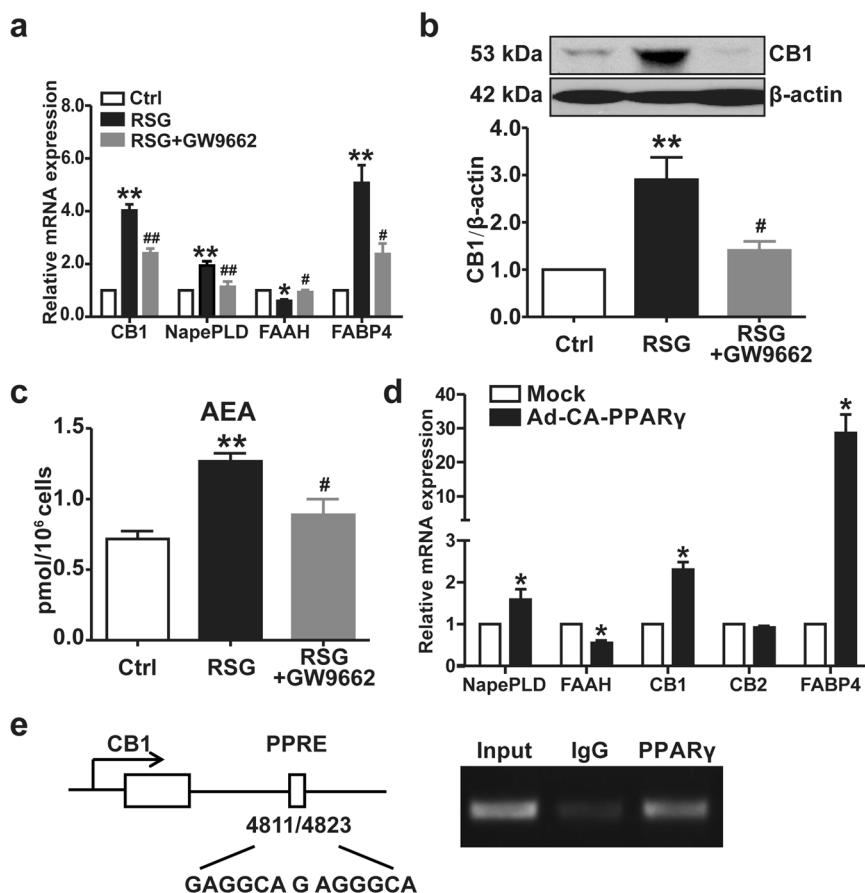


Fig. 3 RSG activated ECS via PPAR γ activation. NCMCs were pretreated with GW9662 ($40 \mu\text{mol} \cdot \text{L}^{-1}$) for 2 h and subjected to RSG ($20 \mu\text{mol} \cdot \text{L}^{-1}$) for 24 or 48 h. **a** After treated with RSG for 24 h, the mRNA relative expression levels of CB1, NapePLD, FAAH, and FABP4 were measured and normalized to Ctrl. **b** Protein levels of CB1 were analyzed after 48 h of treatment. NCMCs lysates were immunoblotted with the antibody of CB1 and shown as relative fold changes in the bar graph. **c** After treated with RSG for 24 h, the level of AEA was measured by LC-MS and normalized in per 10^6 cardiomyocytes. Data are mean \pm SEM. * $P < 0.05$, ** $P < 0.01$ vs. Ctrl, # $P < 0.05$, ## $P < 0.01$ vs. RSG from one-way ANOVA followed by Sidak's *post hoc* tests. $n = 3$ –8. **d** NCMCs were co-infected with Ad-CA-PPAR γ and Ad-tTA with or without tetracycline (Tc, $1 \mu\text{g} \cdot \text{mL}^{-1}$) for 36 h, and the mRNA expression level of related genes was measured. Data are mean \pm SEM. * $P < 0.05$ vs. Mock from *t*-test. $n = 3$. **e** NCMCs were treated with RSG ($20 \mu\text{mol} \cdot \text{L}^{-1}$) for 24 h, then cross-linked and immunoprecipitated with the antibody of PPAR γ or IgG. The immunoprecipitates or supernatants before immunoprecipitation (Input) were PCR amplified using the primers flanking the motifs in the rat CB1 gene.

($20 \mu\text{mol} \cdot \text{L}^{-1}$) increased the mRNA expression levels of ANP and BNP (Fig. 5a, b). In addition, RSG increased the phosphorylation level of mTOR and its downstream protein, 4EBP1, after 48 h of treatment (Fig. 5c). As a target gene of PPAR γ , CB1 may contribute to RSG-induced cardiac hypertrophy. We tested this hypothesis in NCMCs by using the selective CB1 antagonists Rimo and AM251. Both Rimo ($3 \mu\text{mol} \cdot \text{L}^{-1}$) and AM251 ($5 \mu\text{mol} \cdot \text{L}^{-1}$) attenuated the RSG-induced increases in the mRNA expression levels of ANP and BNP (Fig. 5d). Next, we measured the size of cardiomyocytes by rhodamine-conjugated phalloidin staining (Fig. 5e). The results revealed that inhibition of CB1 reduced RSG-stimulated cell hypertrophy. In addition, Rimo inhibited mTOR signaling activation induced by RSG (Fig. 5f). We also investigated whether CB2 is involved in RSG-mediated cardiac hypertrophy. NCMCs were pretreated with the selective CB2 antagonists SR144528 ($1 \mu\text{mol} \cdot \text{L}^{-1}$) and AM630 ($1 \mu\text{mol} \cdot \text{L}^{-1}$) and were then treated with RSG ($20 \mu\text{mol} \cdot \text{L}^{-1}$) for 48 h, and the activation of the mTOR pathway was analyzed by Western blotting. As shown in Fig. S3, neither SR144528 nor AM630 affected mTOR signaling, indicating that CB2 is not involved in RSG-induced myocardial hypertrophy.

For the *in vivo* study, SD rats were administered RSG ($15 \text{mg} \cdot \text{kg}^{-1} \cdot \text{d}^{-1}$) with or without Rimo ($10 \text{mg} \cdot \text{kg}^{-1} \cdot \text{d}^{-1}$) by intragastric gavage for 4 weeks. Analyses of cardiac morphometry

and the expression of molecular markers for cardiac hypertrophy were performed. As shown in Fig. 6, RSG administration markedly increased the heart weight, expressed as the heart-to-body weight ratio (HW/BW) or left ventricle-to-body weight ratio (LVW/BW), and this increase was attenuated by Rimo administration (Fig. 6a–c). Rimo also decreased the cross-sectional area of cardiomyocytes, which was increased by RSG treatment (Fig. 6d, e). Furthermore, Rimo decreased the mRNA expression levels of ANP and BNP and inhibited RSG-induced mTOR pathway activation in heart tissues (Fig. 6f, g). These results thus indicated that the activated cardiac ECS is essential for RSG-induced cardiac hypertrophy.

DISCUSSION

In the present study, we demonstrated that the ECS is an important mediator of the hypertrophic effects of RSG. Activation of PPAR γ induced ECS activation, which was characterized by increased levels of eCBs, altered regulation of key enzymes in eCB biometabolism, and upregulated expression of CB1, in turn leading to cardiac hypertrophic remodeling. Furthermore, we revealed that the CB1 antagonist Rimo suppressed RSG-induced cardiac hypertrophy in both *in vitro* and *in vivo* studies.

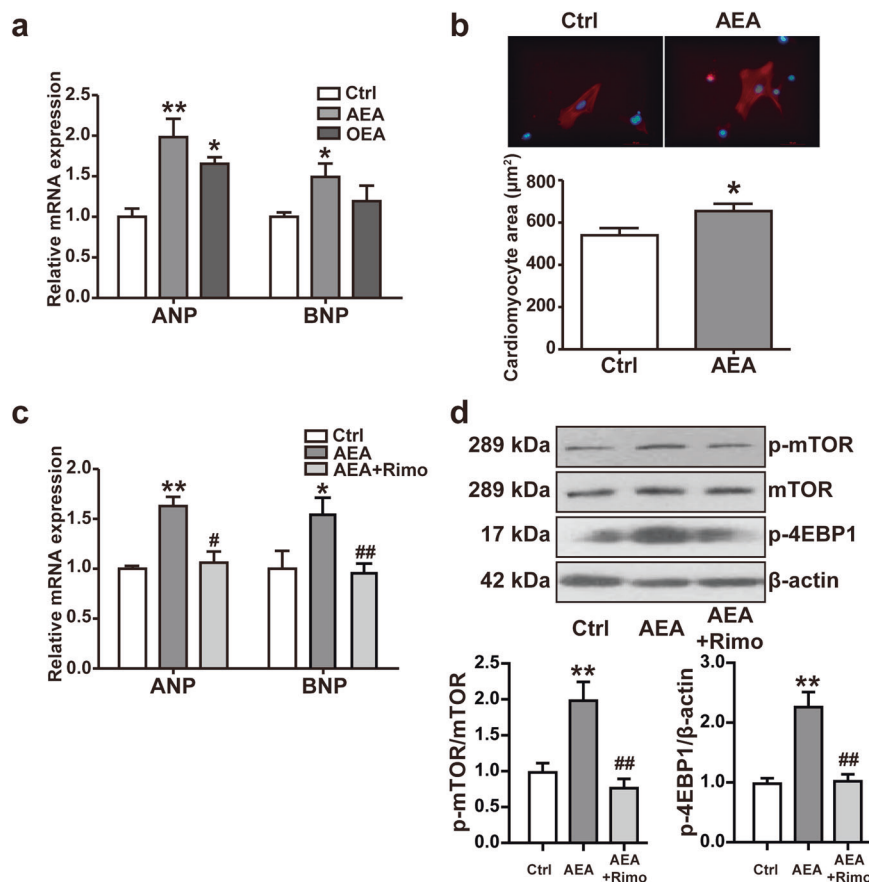


Fig. 4 eCBs exerted hypertrophic effects on NCMCs via CB1. **a** NCMCs were treated with AEA ($10 \mu\text{mol} \cdot \text{L}^{-1}$) or OEA ($50 \mu\text{mol} \cdot \text{L}^{-1}$) for 24 h. The relative mRNA expression levels of ANP and BNP were measured and normalized to Ctrl. Data are mean \pm SEM. * $P < 0.05$, ** $P < 0.01$ vs. Ctrl from one-way ANOVA followed by Sidak's *post hoc* tests. $n = 4$. **b** The F-actin of NCMCs was stained with rhodamine-conjugated phalloidin. The cardiomyocyte area was digitized and the areas (μm^2) of 100 cells from each treatment were determined using Image J. Data are mean \pm SEM. * $P < 0.05$ vs. Ctrl from *t*-test. $n = 6$. **c** NCMCs were pretreated with Rimo ($3 \mu\text{mol} \cdot \text{L}^{-1}$) for 2 h and then subjected to AEA ($10 \mu\text{mol} \cdot \text{L}^{-1}$) for 24 h. The relative mRNA expression levels of ANP and BNP were determined by qPCR. Data are mean \pm SEM. * $P < 0.05$, ** $P < 0.01$ vs. Ctrl, # $P < 0.05$, ## $P < 0.01$ vs. AEA from one-way ANOVA followed by Sidak's *post hoc* tests. $n = 3-7$. **d** After 48 h treatment as indicated, NCMCs were collected for determining protein level by Western blotting. Data are mean \pm SEM. ** $P < 0.01$ vs. Ctrl, ## $P < 0.01$ vs. AEA from one-way ANOVA followed by Sidak's *post hoc* tests. $n = 4$.

We observed opposite effects of RSG stimulation on the AEA and 2-AG levels in cardiomyocytes (Fig. 1). The changes in the levels of these two eCBs were most likely caused by the altered expression of critical enzymes involved in eCB metabolism. Our results showed that TZDs inhibit the expression of FAAH in a PPAR γ -dependent manner (Figs. 2 and 3), contributing to the accumulation of AEA. Although FAAH can catalyze the degradation of both AEA and 2-AG, a recent report showed that FAAH inactivation can increase the level of AEA in tissues and reduce the 2-AG level [48], consistent with our data. It is worth noting that another family of enzymes, namely, monoacylglycerol lipases (MAGLs), are the major contributors to 2-AG degradation, possibly explaining the differential regulation of these two eCBs. We also demonstrated that inhibition of FAAH with its selective inhibitor URB597 in cardiomyocytes caused an increase in the AEA level and a decrease in the 2-AG level (Fig. S4). Functionally, AEA and 2-AG have historically shown opposite effects in cardiovascular disorders. During myocardial ischemia/reperfusion (I/R) injury, 2-AG but not AEA provided protection by reducing the infarct size and myocardial damage [3, 12, 49]. In diabetes- and doxorubicin-induced cardiomyopathy, the AEA level but not the 2-AG level was elevated in cardiac tissue [9, 11]. Previous studies have demonstrated that AEA can inhibit intracellular calcium signaling, leading to hypotension and decreased cardiac contraction [50–52], and the abnormal calcium homeostasis induced by a constantly increasing AEA level may initiate compensatory

hypertrophy in cardiomyocytes [53]. Consistent with this hypothesis, the attenuated activity of FAAH was reported in doxorubicin-induced myocardial tissue injury [54]. This finding was further supported by our results in this study, which showed that treating cardiomyocytes with AEA increased the expression of cardiac hypertrophy markers and the phosphorylation of mTOR and 4EBP1 (Fig. 4). Hence, we can speculate that both an increase in AEA and a decrease in 2-AG may contribute to the adverse myocardial effects of RSG.

Our results showed that ECS activation induced by PPAR γ agonists was likely to be mediated via the AEA/CB1 axis, as demonstrated by the upregulated expression of CB1 but an unchanged expression of CB2 (Figs. 2, 3 and S2). Notably, the CB1-binding activity of AEA was 24 times more potent than that of 2-AG, while 2-AG had a higher affinity for CB2 than did AEA [45]. In line with our findings, the activating AEA/CB1 axis has been characterized in a variety of animal models with cardiac dysfunction. In most studies, CB1 is upregulated in the cardiovascular system under pathological conditions, and inhibition of CB1 is cardioprotective against I/R injury, myocardial ischemia, heart failure, and cardiomyopathies. Conversely, the predominant experimental evidence indicates that activation of CB2 shows beneficial effects in cardiomyocytes [55, 56]. Moreover, we demonstrated that Rimo attenuated RSG-induced cardiac hypertrophy in both primary cardiomyocytes and rat models (Figs. 5, 6).

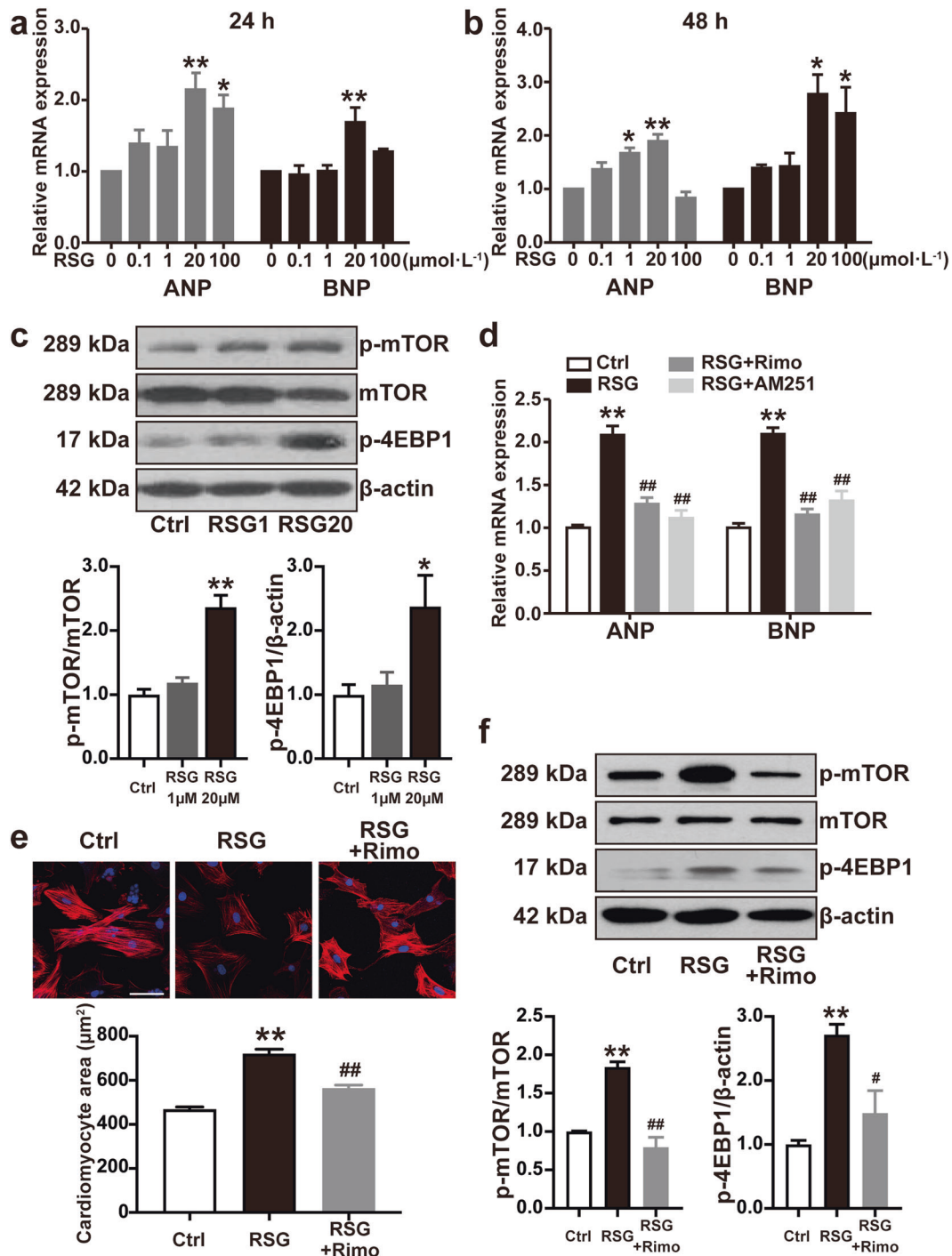


Fig. 5 CB1 antagonist attenuated RSG-induced cardiac hypertrophy in NCMCs. **a, b** NCMCs were treated with the indicated dose of RSG for 24 or 48 h. The relative mRNA expression levels of ANP and BNP were measured and normalized to Ctrl. Data are mean \pm SEM. * P < 0.05, ** P < 0.01 vs. RSG (0 $\mu\text{mol} \cdot \text{L}^{-1}$) from one-way ANOVA followed by Sidak's *post hoc* tests. n = 3–4. **c** The lysates from NCMCs treated with RSG for 48 h were immunoblotted with the indicated antibody for mTOR pathway. Data are mean \pm SEM. * P < 0.05, ** P < 0.01 vs. Ctrl from one-way ANOVA followed by Sidak's *post hoc* tests. n = 4. RSG1, RSG 1 $\mu\text{mol} \cdot \text{L}^{-1}$; RSG20, RSG 20 $\mu\text{mol} \cdot \text{L}^{-1}$. **d** NCMCs were pretreated with Rimo (3 $\mu\text{mol} \cdot \text{L}^{-1}$) or AM251 (5 $\mu\text{mol} \cdot \text{L}^{-1}$) and then subjected to RSG (20 $\mu\text{mol} \cdot \text{L}^{-1}$) for 24 h. The relative mRNA expression levels of ANP and BNP were measured and normalized to Ctrl. Data are mean \pm SEM. ** P < 0.01 vs. Ctrl, ## P < 0.01 vs. RSG from one-way ANOVA followed by Sidak's *post hoc* tests. n = 4. **e** NCMCs were pretreated with Rimo (3 $\mu\text{mol} \cdot \text{L}^{-1}$) for 2 h and then subjected to RSG (20 $\mu\text{mol} \cdot \text{L}^{-1}$) for 48 h. The cardiomyocyte size was measured using rhodamine-phalloidin staining. A total of 100 cells were counted for statistical analysis. Scale bar = 50 μm . Data are mean \pm SEM. ** P < 0.01 vs. Ctrl, ## P < 0.01 vs. RSG from one-way ANOVA followed by Sidak's *post hoc* tests. n = 3. **f** After 48 h treatment as indicated, the cell lysate was immunoblotted with the indicated antibody for the mTOR pathway. Data are mean \pm SEM. ** P < 0.01 vs. Ctrl, # P < 0.05, ## P < 0.01 vs. RSG from one-way ANOVA followed by Sidak's *post hoc* tests. n = 3.

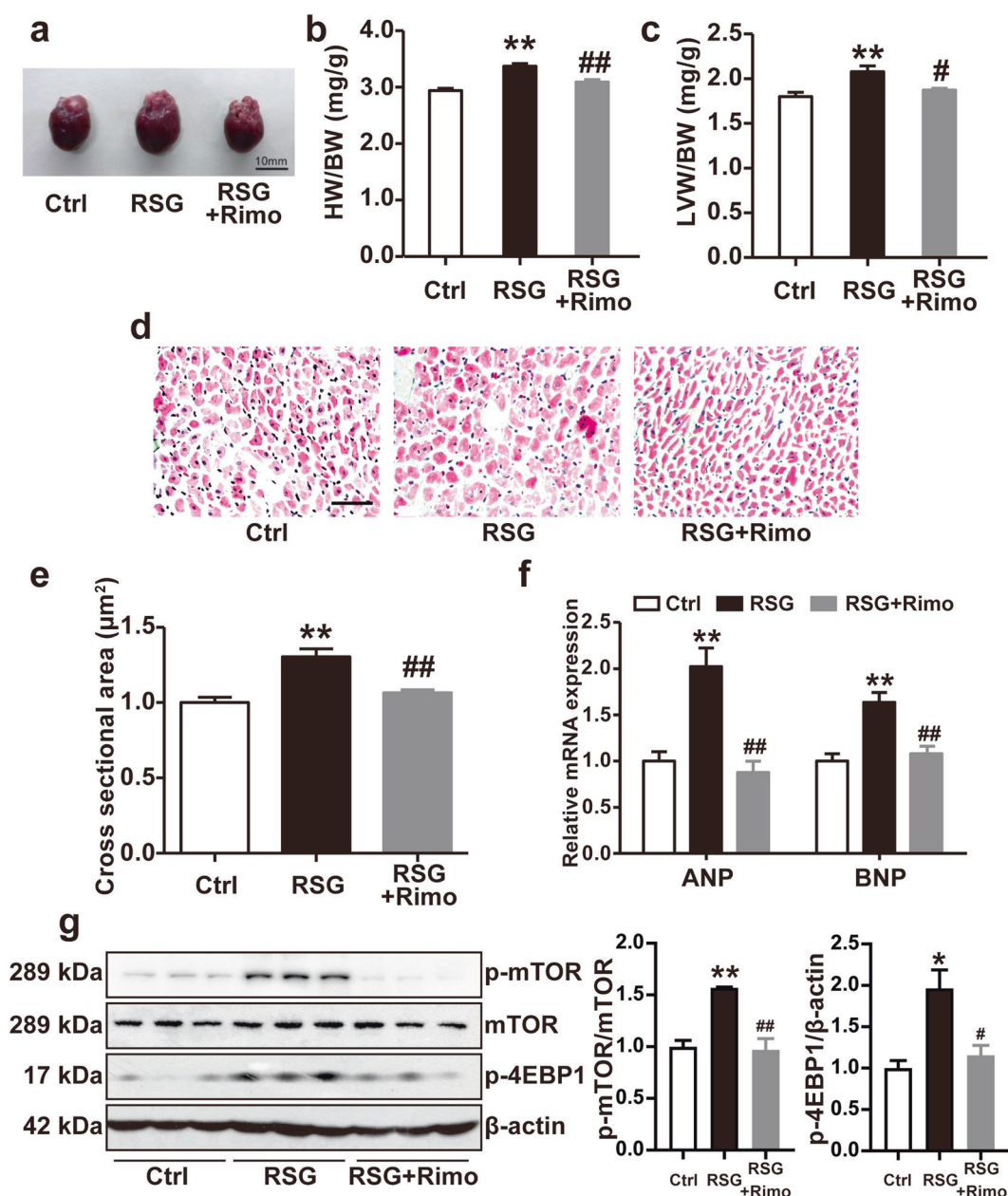


Fig. 6 CB1 antagonist attenuated RSG-induced cardiac hypertrophy in rats. SD rats were treated with RSG (15 mg · kg⁻¹ · d⁻¹) alone or combined with Rimo (10 mg · kg⁻¹ · d⁻¹) by gavage for 4 weeks. **a** Representative photograph of hearts from each group. **b, c** The hearts and left ventricles were weighed and normalized to body weight. **d, e** Histological analysis by HE staining in the cross-section of cardiac tissue. Scale bar = 50 µm. The relative cross-sectional areas of cardiomyocytes were calculated by Image J. **f** The relative mRNA expression levels of ANP and BNP in left ventricles were measured and normalized to Ctrl. **g** The lysate from the left ventricular was immunoblotted with the indicated antibody for the mTOR pathway. Data are mean ± SEM. **P* < 0.05, ***P* < 0.01 vs. Ctrl, #*P* < 0.05, ##*P* < 0.01 vs. RSG from one-way ANOVA followed by Sidak's *post hoc* tests. *n* = 3–8.

In contrast, inhibition of CB2 by using the selective antagonists SR144528 and AM630 had no effects on RSG-induced mTOR signaling (Fig. S3). As a selective CB1 antagonist, Rimo resulted in weight loss and significant improvements in multiple cardiometabolic risk factors [57]. Moreover, Rimo has been proven to exert various direct benefits on cardiac tissue. In the H9C2 myocardial cell line, Rimo attenuated uremic toxin-induced fibrotic effects and reduced doxorubicin-induced apoptosis [7, 10]. In mouse models of type 1 diabetes and hepatic cirrhosis, Rimo promoted cardiac function and attenuated cardiac remodeling [8, 9]. In addition, chronic treatment with Rimo reduced the infarct size in mice after

acute I/R injury [58]. This evidence explains the results that CB1 rather than CB2 is involved in RSG-induced cardiac hypertrophy.

In addition to the increase in the AEA level, we also observed an increase in the OEA level induced by TZDs, along with a slight increase in PEA, but this increase was not significant (Fig. 1). FAAH is responsible for the hydrolysis of other fatty acid amides, including OEA and PEA, which are endocannabinoid-like molecules, as evidenced by the reduced rates of AEA, OEA, and PEA hydrolysis in FAAH^{-/-} mice [44]. It has been reported that PEA can increase the AEA level by competing with AEA for FAAH [59], raising the possibility that PEA is degraded more readily than AEA, which may

explain the nonsignificant increase in PEA. Similar to AEA, OEA also induced the expression of the hypertrophy marker ANP; however, OEA did not induce BNP expression (Fig. 4). Although ANP and BNP perform almost identical biological functions, differential regulation of these two hormones has been found in individuals with different degrees of heart failure. In contrast to ANP mRNA expression, which is already elevated in the early stages of heart failure, cardiac BNP mRNA expression is more specifically induced in overt heart failure, indicating that slightly impaired ventricular function is a powerful stimulus for ANP mRNA induction, while a stronger stimulus might be required for BNP induction [60]. According to this evidence, it is possible that compared with AEA, OEA was a mild stimulant that induced only ANP expression. Moreover, unlike AEA, OEA acted independently of the cannabinoid pathway. The underlying mechanisms of the OEA-mediated hypertrophic effects are worthy of further study.

Although the major role of PPAR γ in lipid metabolism has been well established in recent decades, only a few studies have discussed whether PPAR γ is involved in the regulation of cell membrane lipid signaling. eCBs are endogenous lipid-signaling molecules that are produced in the cell membrane from phospholipid precursors [45]. Our study found that PPAR γ activation systemically stimulated ECS activation by targeting both its endogenous ligand (AEA) and receptor (CB1) in cardiomyocytes. The first component in the response of the ECS to PPAR γ activation was CB1, whose expression was increased by RSG-induced PPAR γ activation in the short term (4 h) and continued to increase over the next 48 h. On the other hand, an increase in AEA was found after 24 h of RSG treatment, because it took a longer time (more than 12 h) to inhibit FAAH expression induced by PPAR γ activation. Considering that GW9662 blocked activation of the ECS by RSG and that PPAR γ bound to the CB1 promoter, we concluded that CB1 is a novel target gene of PPAR γ and that activation of the ECS by TZDs depends on PPAR γ activation. Future studies on the interaction between PPAR γ and ECS can be expanded to other tissues with abundant PPAR γ expression, such as adipose tissue. In differentiated 3T3-L1 cells, we found an effect similar to that described here: RSG increased CB1 expression and decreased FAAH expression (data not shown). Thus, it is possible that the PPAR γ -CB1 axis in adipose tissue may also contribute to the cardiac phenotype.

The mTOR pathway is well known as an essential mediator of cardiac remodeling, since activation of the mTOR signaling pathway increases myofibrillar protein synthesis [61, 62]. Pharmacological inhibition with rapamycin blocks the induction of the hypertrophic phenotype by various factors, including RSG [63–65]. Here, we confirmed that RSG activated the mTOR pathway in primary cardiomyocytes at a concentration of 20 $\mu\text{mol} \cdot \text{L}^{-1}$, accompanied by increased expression of the hypertrophy markers ANP and BNP. Furthermore, it has been reported that cerebral and gastric CB1 activation triggers the mTOR pathway [66, 67]. In this study, we proved that CB1 blockade inhibited RSG-induced mTOR activation in both in vitro and in vivo models, suggesting that CB1 mediates the activation of mTOR by RSG in the heart. This finding identified CB1 as the missing piece linking RSG and mTOR and established a new AEA/CB1/mTOR axis, which is regulated by PPAR γ in the pathogenesis of RSG-induced cardiac remodeling.

In conclusion, our results suggested that ECS is a novel target of PPAR γ in cardiomyocytes. Aberrant activation of the AEA/CB1/mTOR axis mediates RSG-induced cardiac remodeling. Hence, our study provided a new possible explanation for RSG-related cardiovascular risk, which might help to manage and minimize the adverse myocardial effects of RSG.

ACKNOWLEDGEMENTS

This study was supported by grants from the National Key R&D Program of China [2018YFA0800600] and National Science Foundation of China [81830015, 82170422 and 81670408].

AUTHOR CONTRIBUTIONS

NPW and YHL conceived the study and designed the experiments. YHL, YL, XZ, and BLZ performed the experiments. LF helped perform analysis. NPW, YHL, and YL wrote the manuscript.

ADDITIONAL INFORMATION

Supplementary information The online version contains supplementary material available at <https://doi.org/10.1038/s41401-022-00858-x>.

Competing interests: The authors declare no competing interests.

REFERENCES

- Engeli S, Böhnke J, Feldpausch M, Gorzelnik K, Janke J, Bätkei S, et al. Activation of the peripheral endocannabinoid system in human obesity. *Diabetes*. 2005;54:2838–43.
- Singla S, Sachdeva R, Mehta JL. Cannabinoids and atherosclerotic coronary heart disease. *Clin Cardiol*. 2012;35:329–35.
- Alfulaj N, Meiners F, Michalek J, Small-Howard AL, Turner HC, Stokes AJ. Cannabinoids, the heart of the matter. *J Am Heart Assoc*. 2018;7:e009099.
- Sarzani R. Endocannabinoids, blood pressure and the human heart. *J Neuroendocrinol*. 2008;20:58–62.
- Montecucco F, Di Marzo V. At the heart of the matter: the endocannabinoid system in cardiovascular function and dysfunction. *Trends Pharmacol Sci*. 2012;33:331–40.
- Duerr GD, Heinemann JC, Dunkel S, Zimmer A, Lutz B, Lerner R, et al. Myocardial hypertrophy is associated with inflammation and activation of endocannabinoid system in patients with aortic valve stenosis. *Life Sci*. 2013;92:976–83.
- Mukhopadhyay P, Bätkei S, Rajesh M, Czifra N, Harvey-White J, Haskó G, et al. Pharmacological inhibition of CB1 cannabinoid receptor protects against doxorubicin-induced cardiotoxicity. *J Am Coll Cardiol*. 2007;50:528–36.
- Bätkei S, Mukhopadhyay P, Harvey-White J, Kechrid R, Pacher P, Kunos G. Endocannabinoids acting at CB1 receptors mediate the cardiac contractile dysfunction in vivo in cirrhotic rats. *Am J Physiol-Heart Circ Physiol*. 2007;293:H1689–H95.
- Rajesh M, Bätkei S, Kechrid M, Mukhopadhyay P, Lee W-S, Horváth B, et al. Cannabinoid 1 receptor promotes cardiac dysfunction, oxidative stress, inflammation, and fibrosis in diabetic cardiomyopathy. *Diabetes*. 2012;61:716–27.
- Lin C-Y, Hsu Y-J, Hsu S-C, Chen Y, Lee H-S, Lin S-H, et al. CB1 cannabinoid receptor antagonist attenuates left ventricular hypertrophy and Akt-mediated cardiac fibrosis in experimental uremia. *J Mol Cell Cardiol*. 2015;85:249–61.
- Mukhopadhyay P, Rajesh M, Bätkei S, Patel V, Kashiwaya Y, Liaudet L, et al. CB1 cannabinoid receptors promote oxidative stress and cell death in murine models of doxorubicin-induced cardiomyopathy and in human cardiomyocytes. *Cardiovasc Res*. 2009;cvp369.
- Lepicier P, Bouchard JF, Lagneux C, Lamontagne D. Endocannabinoids protect the rat isolated heart against ischaemia. *Br J Pharmacol*. 2003;139:805–15.
- Montecucco F, Lenglet S, Braunersreuther V, Burger F, Pelli G, Bertolotto M, et al. CB(2) cannabinoid receptor activation is cardioprotective in a mouse model of ischemia/reperfusion. *J Mol Cell Cardiol*. 2009;46:612–20.
- Defer N, Wan J, Souktani R, Escoubet B, Perier M, Caramelle P, et al. The cannabinoid receptor type 2 promotes cardiac myocyte and fibroblast survival and protects against ischemia/reperfusion-induced cardiomyopathy. *FASEB J*. 2009;23:2120–30.
- Duerr GD, Heinemann JC, Suchan G, Kolobara E, Wenzel D, Geisen C, et al. The endocannabinoid-CB2 receptor axis protects the ischemic heart at the early stage of cardiomyopathy. *Basic Res Cardiol*. 2014;109:425.
- Lehmann JM, Moore LB, Smith-Oliver TA, Wilkison WO, Willson TM, Kliewer SA. An antidiabetic thiazolidinedione is a high affinity ligand for peroxisome proliferator-activated receptor gamma (PPAR gamma). *J Biol Chem*. 1995;270:12953–6.
- Ibrahimi A, Teboul L, Gaillard D, Amri EZ, Ailhaud G, Young P, et al. Evidence for a common mechanism of action for fatty acids and thiazolidinedione antidiabetic agents on gene expression in preadipose cells. *Mol Pharmacol*. 1994;46:1070–6.
- Wang N, Yin R, Liu Y, Mao G, Xi F. Role of peroxisome proliferator-activated receptor-GAMMA in atherosclerosis—an update. *Circ J*. 2011;75:528–35.
- Winterstein A. Rosiglitazone and the risk of adverse cardiovascular outcomes. *Clin Pharmacol Ther*. 2011;89:776–8.
- Nissen SE, Wolski K. Effect of rosiglitazone on the risk of myocardial infarction and death from cardiovascular causes. *N Engl J Med*. 2007;356:2457–71.
- Singh S, Loke YK, Furberg CD. Long-term risk of cardiovascular events with rosiglitazone: a meta-analysis. *JAMA*. 2007;298:1189–95.
- Wallach JD, Wang K, Zhang AD, Cheng D, Grossetta Nardini HK, Lin H, et al. Updating insights into rosiglitazone and cardiovascular risk through shared data: individual patient and summary level meta-analyses. *BMJ*. 2020;368:l7078.

23. Davidson MA, Mattison DR, Azoulay L, Krewski D. Thiazolidinedione drugs in the treatment of type 2 diabetes mellitus: past, present and future. *Crit Rev Toxicol.* 2018;48:52–108.
24. Hunter JJ, Chien KR. Signaling pathways for cardiac hypertrophy and failure. *N Engl J Med.* 1999;341:1276–83.
25. Pharmaceuticals T. Actos [pioglitazone hydrochloride] prescribing information. 2007. <http://www.actos.com/actospro/prescribniginto.aspx>. 2007.
26. GlaxoSmithKline. Avandia (rosiglitazone maleate) [prescribing information]. 2007. http://us.gsk.com/products/assets/us_avandia.pdf.
27. Sena S, Rasmussen IR, Wende AR, McQueen AP, Theobald HA, Wilde N, et al. Cardiac hypertrophy caused by peroxisome proliferator-activated receptor-gamma agonist treatment occurs independently of changes in myocardial insulin signaling. *Endocrinology.* 2007;148:6047–53.
28. Edgley AJ, Thalen PG, Dahllof B, Lanne B, Ljung B, Oakes ND. PPARgamma agonist induced cardiac enlargement is associated with reduced fatty acid and increased glucose utilization in myocardium of Wistar rats. *Eur J Pharmacol.* 2006;538:195–206.
29. Duan SZ, Ivashchenko CY, Russell MW, Milstone DS, Mortensen RM. Cardiomyocyte-specific knockout and agonist of peroxisome proliferator-activated receptor-gamma both induce cardiac hypertrophy in mice. *Circ Res.* 2005;97:372–9.
30. Bouaboula M, Hilairat S, Marchand J, Fajas L, Le Fur G, Casellas P. Anandamide induced PPARgamma transcriptional activation and 3T3-L1 preadipocyte differentiation. *Eur J Pharmacol.* 2005;517:174–81.
31. Ahn S, Yi S, Seo WJ, Lee MJ, Song YK, Baek SY, et al. A cannabinoid receptor agonist N-arachidonoyl dopamine inhibits adipocyte differentiation in human mesenchymal stem cells. *Biomol Ther.* 2015;23:218–24.
32. Roche M, Kelly JP, O'Driscoll M, Finn DP. Augmentation of endogenous cannabinoid tone modulates lipopolysaccharide-induced alterations in circulating cytokine levels in rats. *Immunology.* 2008;125:263–71.
33. O'Sullivan SE, Kendall DA, Randall MD. Time-dependent vascular effects of Endocannabinoids mediated by peroxisome proliferator-activated receptor gamma (PPARgamma). *PPAR Res.* 2009;2009:425289.
34. Rockwell CE, Snider NT, Thompson JT, Vanden Heuvel JP, Kaminski NE. Interleukin-2 suppression by 2-arachidonoyl glycerol is mediated through peroxisome proliferator-activated receptor gamma independently of cannabinoid receptors 1 and 2. *Mol Pharmacol.* 2006;70:101–11.
35. Zhang J, Hu M, Teng Z, Tang YP, Chen C. Synaptic and cognitive improvements by inhibition of 2-AG metabolism are through upregulation of microRNA-188-3p in a mouse model of Alzheimer's disease. *J Neurosci.* 2014;34:14919–33.
36. Li L, Zhang Z-G, Lei H, Wang C, Wu L-P, Wang J-Y, et al. Angiotensin II reduces cardiac AdipoR1 expression through AT1 receptor/ROS/ERK1/2/c-Myc pathway. *PLoS ONE.* 2013;8:e49915.
37. Wang X, Liu X, Zhan Y, LaVallie ER, DiBlasio-Smith L, Collins-Racie L, et al. Pharmacogenomic, physiological, and biochemical investigations on safety and efficacy biomarkers associated with the peroxisome proliferator-activated receptor-gamma activator rosiglitazone in rodents: a translational medicine investigation. *J Pharmacol Exp Ther.* 2010;334:820–9.
38. Liu Y, Yan X, Mao G, Fang L, Zhao B, Liu Y, et al. Metabonomic profiling revealed an alteration in purine nucleotide metabolism associated with cardiac hypertrophy in rats treated with thiazolidinediones. *J Proteome Res.* 2013;12:5634–41.
39. Mao G, Liu Y, Fang X, Liu Y, Fang L, Lin L, et al. Tumor-derived microRNA-494 promotes angiogenesis in non-small cell lung cancer. *Angiogenesis.* 2015;18:373–82.
40. Pachter P, Bátkai S, Osei-Hyiaman D, Offertaler L, Liu J, Harvey-White J, et al. Hemodynamic profile, responsiveness to anandamide, and baroreflex sensitivity of mice lacking fatty acid amide hydrolase. *Am J Physiol-Heart Circ Physiol.* 2005;289:H533–H41.
41. Han B, Wright R, Kirshhoff AM, Chester JA, Cooper BR, Davisson VJ, et al. Quantitative LC-MS/MS analysis of arachidonoyl amino acids in mouse brain with treatment of FAAH inhibitor. *Anal Biochem.* 2013;432:74–81.
42. Yan B, A J, Hao H, Wang G, Zhu X, Zha W, et al. Metabonomic phenotype Identification of "heart blood stasis obstruction pattern" and "qi and yin deficiency pattern" of myocardial ischemia rat models. *Sci China C Life Sci.* 2009;52:1081–90.
43. Wang N, Verna L, Chen NG, Chen J, Li H, Forman BM, et al. Constitutive activation of peroxisome proliferator-activated receptor-gamma suppresses pro-inflammatory adhesion molecules in human vascular endothelial cells. *J Biol Chem.* 2002;277:34176–81.
44. Lichtman AH, Hawkins EG, Griffin G, Cravatt BF. Pharmacological activity of fatty acid amides is regulated, but not mediated, by fatty acid amide hydrolase in vivo. *J Pharmacol Exp Ther.* 2002;302:73–9.
45. Basavarajappa BS. Critical enzymes involved in endocannabinoid metabolism. *Protein Pept Lett.* 2007;14:237.
46. Huang JV, Greyson CR, Schwartz GG. PPAR-gamma as a therapeutic target in cardiovascular disease: evidence and uncertainty THEMATIC REVIEW SERIES: new lipid and lipoprotein targets for the treatment of cardiometabolic diseases. *J Lipid Res.* 2012;53:1738–54.
47. Hoffmann BR, El-Mansy MF, Sem DS, Greene AS. Chemical proteomics-based analysis of off-target binding profiles for rosiglitazone and pioglitazone: clues for assessing potential for cardiotoxicity. *J Med Chem.* 2012;55:8260–71.
48. Di Marzo V, Maccarrone M. FAAH and anandamide: is 2-AG really the odd one out? *Trends Pharmacol Sci.* 2008;29:229–33.
49. Cunha P, Romao AM, Mascarenhas-Melo F, Teixeira HM, Reis F. Endocannabinoid system in cardiovascular disorders—new pharmacotherapeutic opportunities. *J Pharm Bioallied Sci.* 2011;3:350–60.
50. Al Kury LT, Voitychuk OI, Ali RM, Galadari S, Yang K-HS, Howarth FC, et al. Effects of endogenous cannabinoid anandamide on excitation-contraction coupling in rat ventricular myocytes. *Cell Calcium.* 2014;55:104–18.
51. Krylatov A, Maslov L, Ermakov SY, Lasukova O, Barzakh E, Crawford D, et al. Significance of cardiac cannabinoid receptors in regulation of cardiac rhythm, myocardial contractility, and electrophysiologic processes in heart. *Biol Bull.* 2007;34:28–35.
52. Oz M, Tchugunova YB, Dunn SM. Endogenous cannabinoid anandamide directly inhibits voltage-dependent Ca²⁺ fluxes in rabbit T-tubule membranes. *Eur J Pharmacol.* 2000;404:13–20.
53. Berridge MJ, Bootman MD, Roderick HL. Calcium signalling: dynamics, homeostasis and remodelling. *Nat Rev Mol Cell Biol.* 2003;4:517–29.
54. Mukhopadhyay P, Horváth B, Rajesh M, Matsumoto S, Saito K, Bátkai S, et al. Fatty acid amide hydrolase is a key regulator of endocannabinoid-induced myocardial tissue injury. *Free Radic Biol Med.* 2011;50:179–95.
55. Garza-Cervantes JA, Ramos-Gonzalez M, Lozano O, Jerjes-Sanchez C, Garcia-Rivas G. Therapeutic applications of cannabinoids in cardiomyopathy and heart failure. *Oxid Med Cell Longev.* 2020;2020:4587024.
56. Kaschina E. Cannabinoid CB1/CB2 receptors in the heart: expression, regulation, and function. In: *Cannabinoids in health and disease. Cannabinoids in Health and Disease.* 2016.
57. Pi-Sunyer FX, Aronne LJ, Heshmati HM, Devin J, Rosenstock J, Group, et al. Effect of rimonabant, a cannabinoid-1 receptor blocker, on weight and cardiometabolic risk factors in overweight or obese patients: RIO-North America: a randomized controlled trial. *JAMA.* 2006;295:761–75.
58. Lim SY, Davidson SM, Yellon DM, Smith CC. The cannabinoid CB1 receptor antagonist, rimonabant, protects against acute myocardial infarction. *Basic Res Cardiol.* 2009;104:781–92.
59. Borrelli F, Izzo AA. Role of acylethanolamides in the gastrointestinal tract with special reference to food intake and energy balance. *Best Pract Res Clin Endocrinol Metab.* 2009;23:33–49.
60. Langenickel T, Pagel I, Hohnel K, Dietz R, Willenbrock R. Differential regulation of cardiac ANP and BNP mRNA in different stages of experimental heart failure. *Am J Physiol Heart Circ Physiol.* 2000;278:H1500–6.
61. Dorn GW. Protein kinase cascades in the regulation of cardiac hypertrophy. *J Clin Invest.* 2005;115:527.
62. Proud CG. Ras, PI3-kinase and mTOR signaling in cardiac hypertrophy. *Cardiovasc Res.* 2004;63:403–13.
63. Festuccia WT, Laplante M, Brûlé S, Houde VP, Achouba A, Lachance D, et al. Rosiglitazone-induced heart remodelling is associated with enhanced turnover of myofibrillar protein and mTOR activation. *J Mol Cell Cardiol.* 2009;47:85–95.
64. McMullen JR, Sherwood MC, Tarnavski O, Zhang L, Dorfman AL, Shioi T, et al. Inhibition of mTOR signaling with rapamycin regresses established cardiac hypertrophy induced by pressure overload. *Circulation.* 2004;109:3050–5.
65. Gao X-M, Wong G, Wang B, Kiriazis H, Moore X-L, Su Y-D, et al. Inhibition of mTOR reduces chronic pressure-overload cardiac hypertrophy and fibrosis. *J Hypertens.* 2006;24:1663–70.
66. Puighermanal E, Marsicano G, Busquets-García A, Lutz B, Maldonado R, Ozaita A. Cannabinoid modulation of hippocampal long-term memory is mediated by mTOR signaling. *Nat Neurosci.* 2009;12:1152–8.
67. Senin LL, Al-Massadi O, Folgueira C, Castela C, Pardo M, Barja-Fernandez S, et al. The gastric CB1 receptor modulates ghrelin production through the mTOR pathway to regulate food intake. *PLoS ONE.* 2013;8:e80339.